Article

TRANSPARENT PROCESS

EMBO reports

Lack of TRPV2 impairs thermogenesis in mouse brown adipose tissue

Wuping Sun[1,2], Kunitoshi Uchida[1,2,*], Yoshiro Suzuki[1,2], Yiming Zhou[1], Minji Kim[3], Yasunori Takayama[1,2], Nobuyuki Takahashi[3], Tsuyoshi Goto[3], Shigeo Wakabayashi[4], Teruo Kawada[3], Yuko Iwata[4] & Makoto Tominaga[1,2,**]

Abstract

Brown adipose tissue (BAT), a major site for mammalian non-shivering thermogenesis, could be a target for prevention and treatment of human obesity. Transient receptor potential vanilloid 2 (TRPV2), a Ca^{2+}-permeable non-selective cation channel, plays vital roles in the regulation of various cellular functions. Here, we show that TRPV2 is expressed in brown adipocytes and that mRNA levels of thermogenic genes are reduced in both cultured brown adipocytes and BAT from TRPV2 knockout (TRPV2KO) mice. The induction of thermogenic genes in response to β-adrenergic receptor stimulation is also decreased in TRPV2KO brown adipocytes and suppressed by reduced intracellular Ca^{2+} concentrations in wild-type brown adipocytes. In addition, TRPV2KO mice have more white adipose tissue and larger brown adipocytes and show cold intolerance, and lower BAT temperature increases in response to β-adrenergic receptor stimulation. Furthermore, TRPV2KO mice have increased body weight and fat upon high-fat-diet treatment. Based on these findings, we conclude that TRPV2 has a role in BAT thermogenesis and could be a target for human obesity therapy.

Keywords BAT; Ca^{2+}; thermogenesis; TRPV2; UCP1
Subject Categories Membrane & Intracellular Transport; Metabolism
DOI 10.15252/embr.201540819 | Received 8 June 2015 | Revised 30 December 2015 | Accepted 13 January 2016 | Published online online 11 February 2016
EMBO Reports (2016) 17: 383–399

Introduction

The prevalence of obesity has increased worldwide, and it is believed to be the result of an imbalance between the intake and expenditure of energy [1]. Obesity is also a serious health problem that is implicated in various diseases including type II diabetes, hypertension, coronary heart diseases, and cancer [2], and it is characterized by increased adipose tissue mass that results from increased fat cell size and number, suggesting that the main contributor to obesity is adipose tissue [3]. Unlike white adipose tissue (WAT), brown adipose tissue (BAT) is specialized for the efficient dissipation of chemical energy in the form of heat, and BAT is a major site for mammalian non-shivering thermogenesis with mitochondrial uncoupling protein 1 (UCP1) [4,5]. Although BAT was originally identified in infants and rodents, recent studies have reported that BAT also exists in adult humans as demonstrated using a combination of high-resolution imaging techniques [6,7]. This novel finding highlights the crucial role for BAT in the regulation of energy metabolism and fat deposition [8,9]. Upon cold exposure or β-adrenergic receptor stimulation, BAT functions are activated and "browning" of WAT occurs as well due to the emerged UCP1-positive "beige" cells [10,11]. When activated, UCP1 in mitochondria uncouples the respiratory chain and heat is generated [12,13]. Moreover, BAT activity in human and the amount of BAT tissue are inversely correlated with adiposity [14]. Thus, BAT could be a promising target for human obesity prevention and treatment, and understanding the molecular mechanisms for thermogenesis in brown adipocytes is the subject of intense investigation.

The concentrations of intracellular Ca^{2+} ($[Ca^{2+}]_i$) and the amplitude of its fluctuations have primary importance for survival and function in a plethora of cell types [15]. For many cells, there have been extensive studies of $[Ca^{2+}]_i$ signals, whereas relatively little knowledge about Ca^{2+} signaling in white and brown adipocytes is available despite its suggested importance [16].

Transient receptor potential vanilloid 2 (TRPV2) is activated by noxious heat with an activation temperature threshold of higher than 52°C [17] and by a number of chemical ligands, for example, 2-aminoethoxydiphenyl borate (2APB) and lysophosphatidylcholine (LPC) in a species-specific manner [18,19]. SKF96365 (SKF) is a TRPV2-selective antagonist [18,20]. Importantly, TRPV2 is also reported to be a mechano-sensitive channel activated by mechanical stretch and cell swelling [21,22]. Several studies have reported the involvement of TRP channels in adipose tissue functions. For example, TRPV1 was reported to be involved in the regulation of food

1 Division of Cell Signaling, Okazaki Institute for Integrative Bioscience (National Institute for Physiological Sciences), Okazaki, Japan
2 Department of Physiological Sciences, SOKENDAI (The Graduate University for Advanced Studies), Okazaki, Japan
3 Division of Food Science and Biotechnology, Graduate School of Agriculture, Kyoto University, Uji, Japan
4 Department of Molecular Physiology, National Cerebral and Cardiovascular Center Research Institute, Suita, Osaka, Japan
*Corresponding author. Tel: +81 564 59 5287/5286; Fax: +81 564 59 5285; E-mail: kuchida@nips.ac.jp
**Corresponding author. Tel: +81 564 59 5287/5286; Fax: +81 564 59 5285; E-mail: tominaga@nips.ac.jp

intake and glucose homeostasis in white fat during obesity [23]. And the roles of TRPV1 and TRPV3 have been shown in the regulation of adipogenesis; their activation-mediated Ca^{2+} influx prevents white adipocyte differentiation and plays anti-adipogenic roles *in vivo* [24,25]. TRPM8 stimulation by its ligands increased UCP1 expression in brown adipocytes and BAT through PKA phosphorylation [26]. Moreover, activation of TRPV1 by capsaicin or TRPM8 by cold temperature or menthol enhanced UCP1 expression [27,28], whereas knockdown of TRPV4 facilitated UCP1 expression in white adipocytes [29]. Although recent studies indicate that the involvement of $[Ca^{2+}]_i$ increases in the functions of adipose tissues [26,29], the roles of Ca^{2+} influx in BAT are still not well understood.

In this study, we demonstrated that TRPV2 was functionally expressed in mouse brown adipocytes in culture. mRNA levels of thermogenic genes were significantly lower in both cultured brown adipocytes and BAT from TRPV2 knockout (TRPV2KO) mice, and increases in the genes in response to β-adrenergic receptor stimulation were significantly lower in TRPV2KO brown adipocytes and significantly suppressed by reduction in intracellular Ca^{2+} concentrations in wild-type (WT) brown adipocytes. More interestingly, TRPV2KO interscapular BAT (iBAT) showed impaired adaptive thermogenesis upon cold exposure and administration of a β3-adrenergic receptor agonist. And TRPV2KO mice showed significantly heavier body weight and fat upon high-fat-diet (HFD) treatment for 8 weeks continuously. These data suggest that regulation of Ca^{2+} influx by TRPV2 is critical for maintaining iBAT thermogenic functions under physiological conditions and stimulation.

Results

TRPV2 was functionally expressed in the differentiated mouse brown adipocytes in culture

To explore the expression pattern of TRP channels in adipocytes, we first examined TRPV2 expression in primary cultured brown adipocytes and BAT. RT–PCR and real-time RT–PCR analyses revealed that the expression level of *Trpv2* mRNA looked the highest in the differentiated mouse brown adipocytes among *Trpv1*, *Trpv2*, *Trpv3*, and *Trpv4* (Fig 1A and B). The same result was obtained in the analysis of mouse iBAT (Fig 1C). The mRNA expression of *Trpm8* was significantly lower than *Trpv2* in iBAT (Fig EV1A). Although *Trpv2* mRNA expression was not different among brown adipocytes, CD11b-negative (CD11b (−)) and CD11b-positive (CD11b (+), macrophages) cells isolated from WT iBAT (Fig EV1B-D), the CD11b (+) fractions were negligibly small compared with brown adipocytes, suggesting the little contribution of macrophages to the BAT functions. We next examined the expression of TRPV2 protein in differentiated brown adipocytes from WT and TRPV2KO mice by Western blotting, and lack of TRPV2 was confirmed in TRPV2KO mice (Fig 1D). Then, we examined the functional expression of TRPV2 in mouse brown adipocytes using Ca^{2+} imaging and whole-cell patch-clamp methods. A TRPV2 agonist, either 2APB or LPC, increased $[Ca^{2+}]_i$ which was blocked by SKF (Fig EV1E and F), indicating that the observed 2APB- or LPC-evoked $[Ca^{2+}]_i$ increases were mediated by TRPV2 activation. Adipocytes showed increases in $[Ca^{2+}]_i$ upon activation of α1-adrenergic receptor by norepinephrine (NE) through Gq-coupled receptor signaling, indicating that they were differentiated adipocytes (Figs 1E and EV1E–G), and such 2APB- or LPC-evoked $[Ca^{2+}]_i$ increases were drastically reduced in TRPV2KO brown adipocytes (Figs 1E and EV1G), further indicating the functional TRPV2 expression in WT differentiated brown adipocytes. Whole-cell patch-clamp recordings showed that 2APB activated currents with outward rectification that was blocked by SKF (Fig 1F). Mean densities of the 2APB-induced currents in mouse brown adipocytes at −60 mV and + 100 mV were significantly smaller in the cells given both 2APB and SKF compared with cells given 2APB alone (Fig 1G). These results demonstrated that TRPV2 is functionally expressed in the differentiated mouse brown adipocytes.

Lack of TRPV2 facilitated brown adipocyte differentiation

In order to examine the involvement of TRPV2 in adipocyte differentiation like TRPV1 and TRPV3 [24,25], we compared the mRNA expression of *Trpv1*, *Trpv2*, *Trpv3*, and *Trpv4* in pre-adipocytes from mouse iBAT and 6-day differentiated brown adipocytes. Only *Trpv2* mRNA level was significantly increased in 6-day differentiated

Figure 1. TRPV2 was functionally expressed in mouse differentiated brown adipocytes.

A RT–PCR analysis of the expression of *β-actin*, *Trpv1*, *Trpv2*, *Trpv3*, and *Trpv4* using mouse differentiated brown adipocytes after 29 (upper) and 35 (lower) thermal cycles with (RT (+)) and without (RT (−)) reverse transcription (RT). Control (Ct.) lanes indicate the results with each plasmid DNA as a template.

B Results of real-time RT–PCR analysis of *Trpv1*, *Trpv2*, *Trpv3*, and *Trpv4* expression using mouse differentiated brown adipocytes. Expression levels of mRNA were normalized to that of the ribosomal protein gene (*36B4*), a housekeeping gene unaffected by adipogenesis. Data are presented as mean ± SEM, $n = 6$.

C Results of real-time PCR analysis of *Trpv1*, *Trpv2*, *Trpv3*, and *Trpv4* expression using mouse interscapular brown adipose tissue (iBAT). mRNA expression levels were normalized to that of *36B4*. Data are presented as mean ± SEM, $n = 5$.

D Western blot results of TRPV2 and tubulin from WT and TRPV2KO brown adipocytes. Upper bands in the TRPV2 blots likely indicate glycosylated forms.

E Averaged traces of $[Ca^{2+}]_i$ changes in response to 500 μmol/l 2APB in differentiated brown adipocytes from WT (black) and TRPV2KO (red) mice. One μmol/l NE was used to confirm differentiation. Five μmol/l ionomycin was used to confirm cell viability. Ratio values correspond to the real $[Ca^{2+}]_i$ of differentiated mouse brown adipocytes. Data are presented as mean ± SEM, $n = 149$ of WT cells, and $n = 112$ of TRPV2KO brown adipocytes; $^{**}P < 0.01$. Unpaired Student's *t*-test.

F A representative trace of whole-cell current activated by 3 mmol/l of 2APB in the presence or absence of 10 μmol/l SKF in mouse differentiated brown adipocyte. The left inset indicates a voltage-ramp pulse protocol. The right inset indicates the current–voltage curves of basal current (a, black), current in the presence of 2APB+SKF (b, blue), and current in the presence of 2APB alone (c, red) at the time points of a, b, and c, respectively.

G Comparison of the mean densities of basal currents (Base, black), currents in the presence of 2APB alone (red), and currents in the presence of 2APB+SKF (blue) at −60 mV and + 100 mV in mouse differentiated brown adipocytes. Data are presented as mean ± SEM, $n = 10$; $^{**}P < 0.01$ vs. Base; $^{\#\#}P < 0.01$ vs. 2APB alone. One-way ANOVA followed by 2-tailed *t*-test with Bonferroni correction.

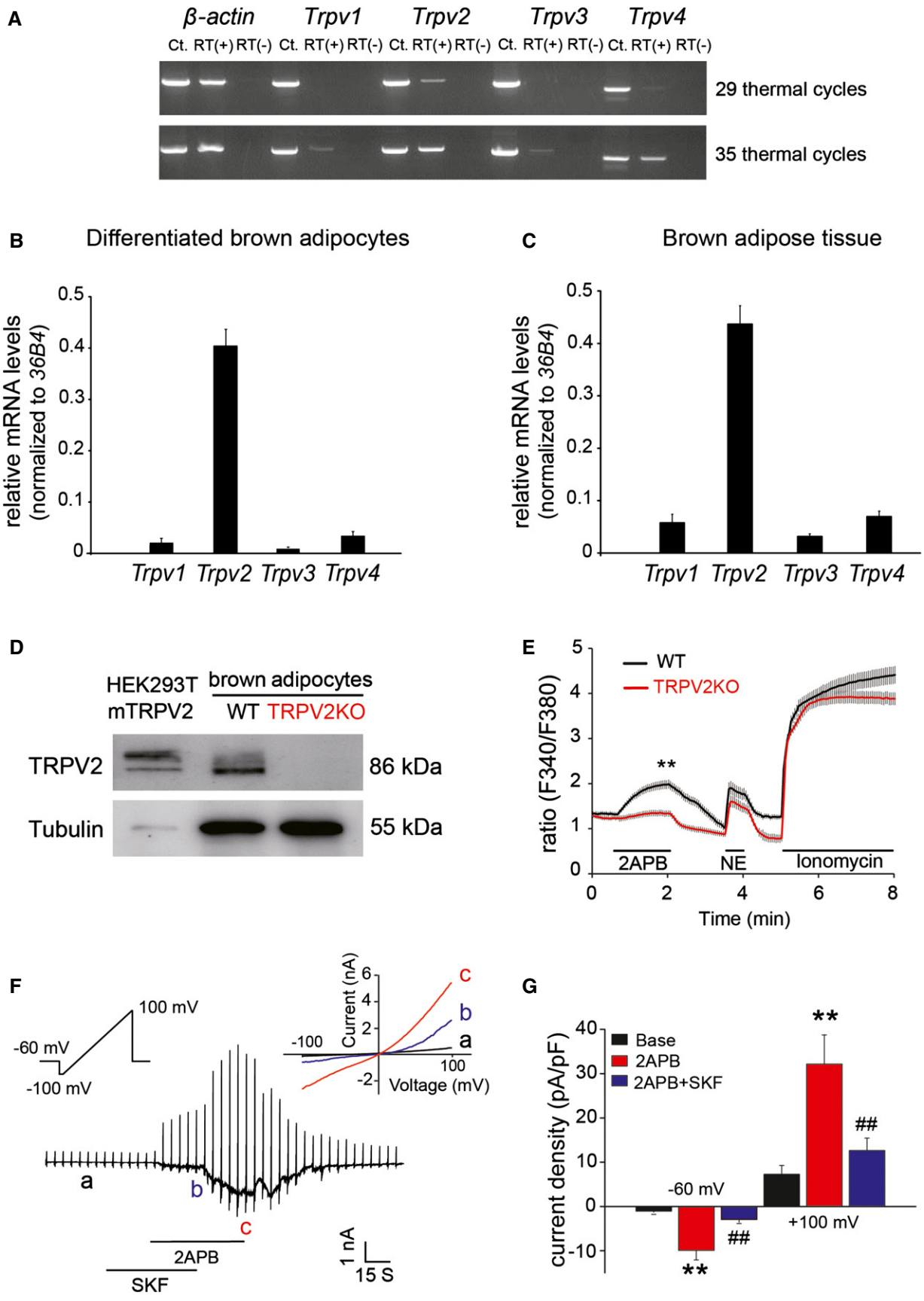

Figure 1.

brown adipocytes (Fig 2A). To further clarify the involvement of TRPV2 in the differentiation and the thermogenic function of mouse brown adipocytes, we analyzed the brown adipocytes from WT and TRPV2KO mice. Continuous treatment with either 2APB or LPC for 6 days significantly reduced the number of differentiated brown adipocytes (Fig 2B). Then, we compared the differentiated brown adipocyte number in WT and TRPV2KO cells. Although number of differentiated brown adipocytes and triglyceride levels were not different between WT and TRPV2KO cells with control differentiation medium, significantly more differentiated brown adipocytes and higher triglyceride levels were observed in TRPV2KO adipocytes when we used ten-time-diluted differentiation medium (Fig 2C and D). These results can be interpreted that differentiation was saturated in the condition with control medium and that the difference became significant in the condition with reduced differentiation efficiency. This TRPV2-dependent brown adipocyte differentiation is consistent with the data shown in Fig 2B. These results demonstrated that TRPV2 could be activated even in the *in vitro* condition and that this activation could prevent mouse brown adipocyte differentiation.

TRPV2-dependent increases in the expression of thermogenic genes could involve intracellular Ca^{2+} signaling in brown adipocytes

Because expression of *Trpv2* was increased in the differentiated brown adipocytes, we also compared mRNA levels of thermogenic genes between WT and TRPV2KO brown adipocytes. *Ucp1* and peroxisome proliferator-activated receptor gamma coactivator 1-alpha (*Pgc1a*) mRNA levels were significantly lower in TRPV2KO brown adipocytes, while peroxisome proliferator-activated receptor γ (*Pparg*) and β3-adrenergic receptor (*Adrb3*) mRNA levels were not different (Fig 3A), suggesting that TRPV2 is involved in the thermogenic function of brown adipocytes. It is known that the mRNA levels of

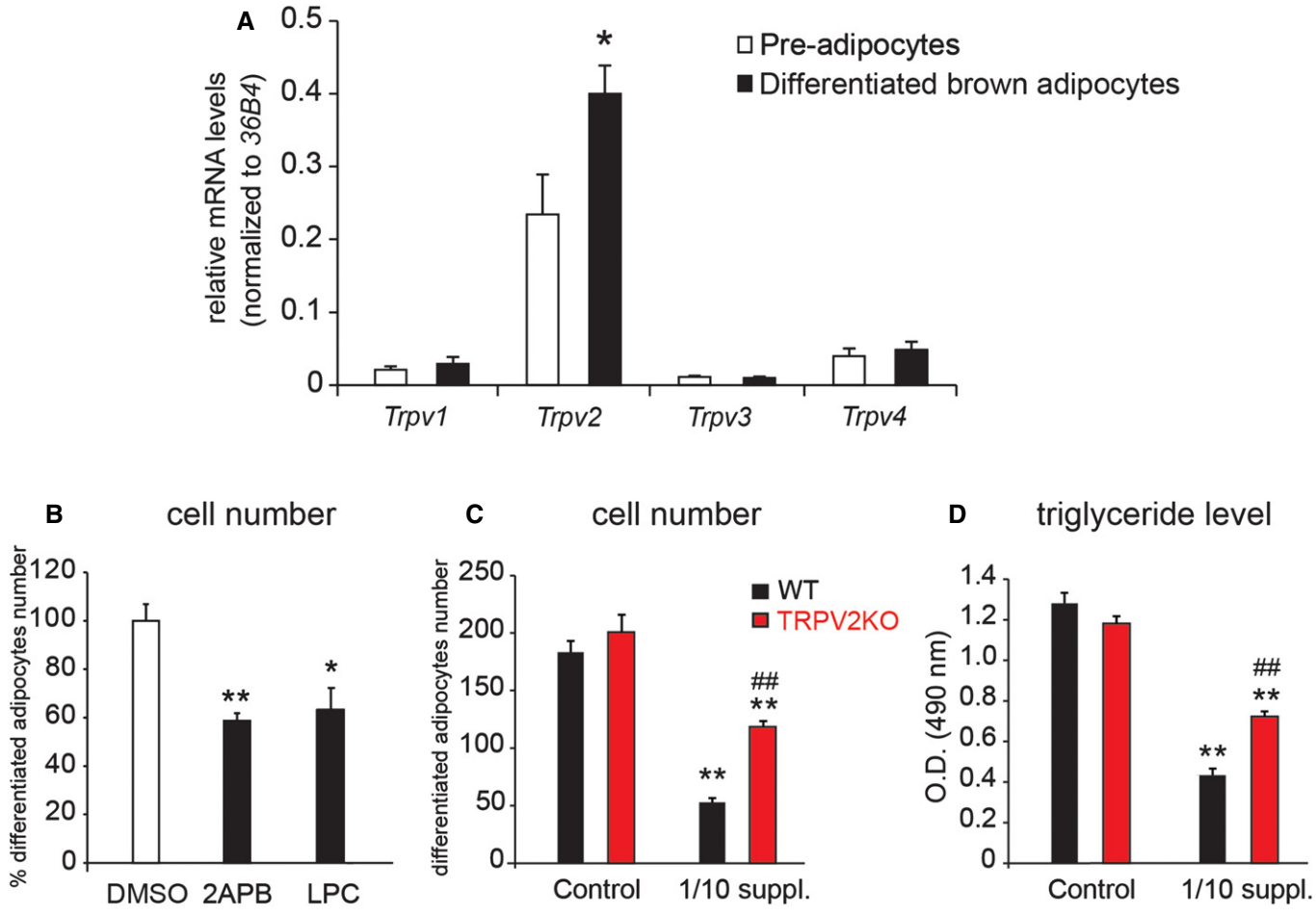

Figure 2. Brown adipocytes from TRPV2KO mice exhibited facilitated differentiation.

A Results of real-time RT–PCR analysis of *Trpv1*, *Trpv2*, *Trpv3*, and *Trpv4* expression in mouse pre-adipocytes and differentiated brown adipocytes. Expression levels of mRNA were normalized to those of *36B4*. Data are presented as mean ± SEM, $n = 6$. $^{*}P < 0.05$ vs. pre-adipocytes. Unpaired Student's *t*-test.

B The number of 6-day differentiated mouse brown adipocytes treated with TRPV2 agonists, 100 μmol/l 2APB or 10 μmol/l LPC. Mean ± SEM, $n = 6$, $^{*}P < 0.05$ and $^{**}P < 0.01$ vs. dimethyl sulfoxide (DMSO) group. One-way ANOVA followed by 2-tailed *t*-test with Bonferroni correction.

C, D Comparison of the numbers of 6-day differentiated mouse brown adipocytes (C) and triglyceride levels (D) in the cells from WT and TRPV2KO mice with different differentiation media. 1/10 suppl. indicates differentiation medium ten-time-diluted with DMEM. Mean ± SEM, $n = 8$, $^{**}P < 0.01$ vs. control group, $^{\#\#}P < 0.01$ vs. WT group. One-way ANOVA followed by 2-tailed *t*-test with Bonferroni correction.

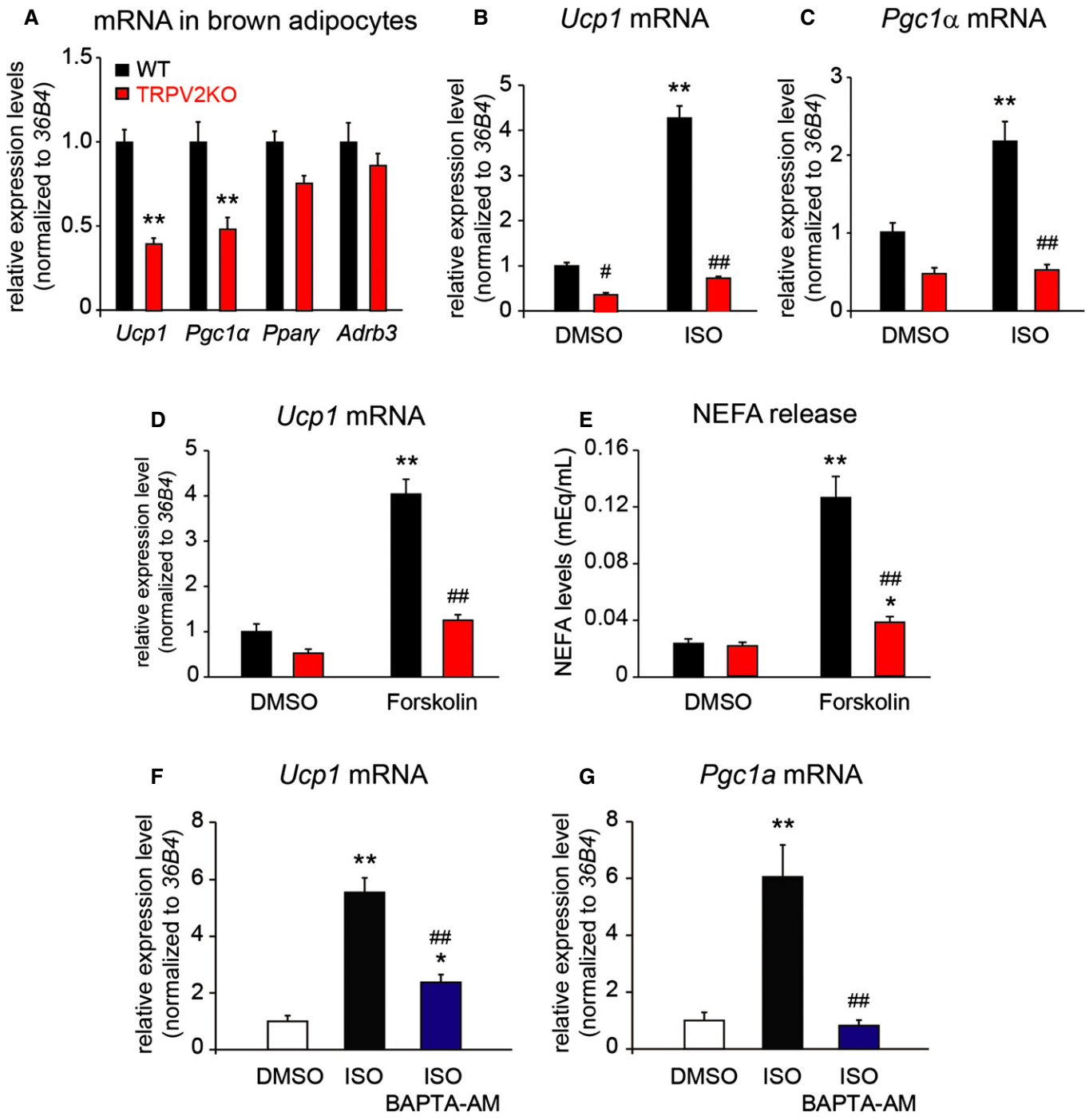

Figure 3. Basal expression of genes related to BAT function and their changes.

A Basal mRNA expression of *Ucp1*, peroxisome proliferator-activated receptor gamma coactivator 1-alpha (*Pgc1a*), peroxisome proliferator-activated receptor γ (*Pparg*), and β-adrenergic receptor 3 (*Adrb3*) in the differentiated brown adipocytes from WT and TRPV2KO mice. Data are presented as mean ± SEM, $n = 5$; $^{**}P < 0.01$ vs. WT. Unpaired Student's *t*-test.

B, C Changes in *Ucp1* (B) and *Pgc1a* (C) mRNA expression in the differentiated brown adipocytes from WT and TRPV2KO mice with and without 10 μmol/l isoproterenol (ISO) for 4 h. Data are presented as mean ± SEM, $n = 5$; $^{**}P < 0.01$ vs. DMSO group; $^{\#}P < 0.05$; $^{\#\#}P < 0.01$ vs. WT group. One-way ANOVA followed by 2-tailed *t*-test with Bonferroni correction.

D, E Changes in *Ucp1* mRNA expression (D) and non-esterified fatty acid (NEFA) release (E) in the differentiated brown adipocytes from WT and TRPV2KO mice with or without 10 μmol/l forskolin for 4 h. Data are presented as mean ± SEM, $n = 6$; $^{*}P < 0.05$; $^{**}P < 0.01$ vs. DMSO group; $^{\#\#}P < 0.01$ vs. WT group. One-way ANOVA followed by 2-tailed *t*-test with Bonferroni correction.

F, G Changes in *Ucp1* mRNA (F) and *Pgc1a* mRNA (G) in the differentiated brown adipocytes treated with 10 μmol/l ISO alone or 10 μmol/l ISO plus 10 μmol/l BAPTA-AM for 4 h. Data are presented as mean ± SEM, $n = 6$; $^{*}P < 0.05$; $^{**}P < 0.01$ vs. DMSO group; $^{\#\#}P < 0.01$ vs. ISO group. One-way ANOVA followed by 2-tailed *t*-test with Bonferroni correction.

Table 1. Blood biochemical parameters and oxygen consumption in WT and TRPV2KO mice.

	Blood glucose (mg/dl)	Plasma insulin (ng/ml)	Serum NEFA (mEq/l)	Serum cholesterol (mg/dl)	Oxygen consumption (ml/kg/h)	
					Dark	Light
WT	157.63 ± 9.79	0.94 ± 0.13	0.91 ± 0.16	58.09 ± 8.69	3804.74 ± 151.62	3044.55 ± 151.21
TRPV2KO	154.50 ± 6.22$^{n.s.}$	1.39 ± 0.27$^{n.s.}$	0.84 ± 0.13$^{n.s.}$	44.52 ± 4.46$^{n.s.}$	4063.26 ± 90.85$^{n.s.}$	2984.90 ± 66.20$^{n.s.}$

NEFA: Non-esterified fatty acid. Data are represented as the mean ± SEM of 8 mice in each group. n.s. indicates that no significant differences were observed between WT and TRPV2KO mice. Unpaired Student's *t*-test.

Ucp1 and *Pgc1a* are enhanced by sympathetic nerve activation after cold exposure [30,31]. Thus, we examined the effect of isoproterenol (ISO), a β-adrenergic receptor agonist, on brown adipocytes. Although WT brown adipocytes exhibited the increases in *Ucp1* and *Pgc1a* mRNA expression levels after ISO treatment, these increases were almost abolished in the TRPV2KO cells (Fig 3B and C). Thus, modulation of the basal expression level of thermogenic genes and the response to β-adrenergic receptor stimuli may be impaired in TRPV2KO brown adipocytes. In order to investigate the pathways downstream of β-adrenergic receptor activation, we examined the effects of forskolin on brown adipocytes. mRNA expression level of *Ucp1* (Fig 3D) and non-esterified fatty acid (NEFA) release (Fig 3E) were significantly enhanced in brown adipocytes from WT mice treated with forskolin. On the other hand, the enhancement was significantly reduced in TRPV2KO brown adipocyte. These results suggested that TRPV2-dependent induction in the expression of thermogenic genes in brown adipocytes involves a cyclic adenosine monophosphate pathway. To test the importance of $[Ca^{2+}]_i$ for the thermogenic gene expression in brown adipocytes, we applied BAPTA-AM, a cell-permeant Ca^{2+} chelator. BAPTA-AM treatment significantly reduced the induction of *Ucp1* and *Pgc1a* mRNA expression by ISO (Fig 3F and G), suggesting that $[Ca^{2+}]_i$ changes possibly due to Ca^{2+} influx through TRPV2 are critical for the induction of thermogenic genes upon activation of sympathetic nervous system.

TRPV2KO mice might have exhibited an energy imbalance

We examined whether TRPV2KO mice exhibited impairments in energy metabolism. Table 1 depicts a comprehensive evaluation of the multiple metabolic parameters in WT and TRPV2KO mice. Under *at libitum* feeding conditions, blood glucose, plasma insulin, NEFA, and serum cholesterol levels were not different between WT and TRPV2KO mice. TRPV2KO mice exhibited significantly smaller body weights until 8 weeks of age (Fig 4A) as previously reported [32]. On the other hand, food intake and water intake were not different between WT and TRPV2KO mice (Fig 4B and C). We then compared the weights of tissues related to energy metabolism upon normalization to their body weights to minimize the effects of body weight difference. The normalized weights of iBAT, iWAT, and epididymal WAT (eWAT) were significantly larger in TRPV2KO mice compared with WT mice at 8 weeks of age (Fig 4D). Moreover, the mRNA levels of *Ucp1* and *Pgc1a* were significantly lower in TRPV2KO iBAT similar to the brown adipocytes (Fig 3A), while *Pparg*, *Adrb3*, cytochrome c oxidase subunit 4 isoform 1 (*Cox4i1*) mRNA levels were not different (Fig 4E). PR domain containing 16 (*Prdm16*) expression was not different, either (Fig 4E), suggesting that differentiation of brown adipocytes is not different in the tissue level. On the other hand, the *Ucp2* expression levels were not different between WT and TRPV2KO iBAT probably because expression levels were very low. Interestingly, the expression levels of genes associated with lipid metabolism (lipoprotein lipase (*Lpl*) and cluster of differentiation 36 (*Cd36*)) were slightly higher in TRPV2KO iBAT although the differences were not significant (Fig 4E). These results suggested that an energy imbalance might have existed in TRPV2KO mice.

Adipocytes from TRPV2KO iBAT exhibited an accumulation of lipid droplets and an increase in cell size

To further explore the involvement of TRPV2 in mouse iBAT function, we performed a histological study by a hematoxylin and eosin staining. Surprisingly, we observed more and larger lipid droplets rather than multiple lipid droplets in adipocytes from 8-week-old TRPV2KO mice (Fig 5A). When comparing the droplet size distribution, mean values were significantly larger in TRPV2KO iBAT in 8-week-old mice compared with WT iBAT (Fig 5B). In addition, cell diameters were also distributed over larger ranges in TRPV2KO adipocytes than in WT cells (Fig 5C), and mean diameters of TRPV2KO adipocytes were significantly larger than those of WT cells (Fig 5D). These data suggested that iBAT "whitening" could have occurred in the iBAT lacking TRPV2. We also examined the iWAT from WT and TRPV2KO mice. mRNA expression of *Trpv2* was not significantly different between inguinal WAT (iWAT) and

Figure 4. Energy imbalance in TRPV2-deficient mice.

A Body weight changes from 3 weeks to 8 weeks of age between the two genotypes (n = 11). Data are presented as mean ± SEM; *P < 0.05; **P < 0.01 vs. WT group. Unpaired Student's *t*-test.

B, C Changes in food intake (B) and water intake (C) from 3 weeks to 8 weeks of age between WT and TRPV2KO mice (n = 6). Data are presented as mean ± SEM.

D Weights of tissues related to energy metabolism normalized to their body weights in WT and TRPV2KO mice (n = 15). Data are presented as mean ± SEM; *P < 0.05; **P < 0.01 vs. WT group. Unpaired Student's *t*-test.

E The expression levels of mRNA related to energy metabolism in iBAT from WT and TRPV2KO mice. mRNA expression levels of *Ucp1*, *Pgc1a*, *Pparg*, *Adrb3*, cytochrome c oxidase subunit 4 isoform 1 (*Cox4i1*), PR domain containing 16 (*Prdm16*), *Ucp2*, lipoprotein lipase (*Lpl*), and cluster of differentiation 36 (*Cd36*) were examined and normalized to the levels of *36B4*. Data are presented as mean ± SEM, n = 15; *P < 0.05 vs. WT group. Unpaired Student's *t*-test.

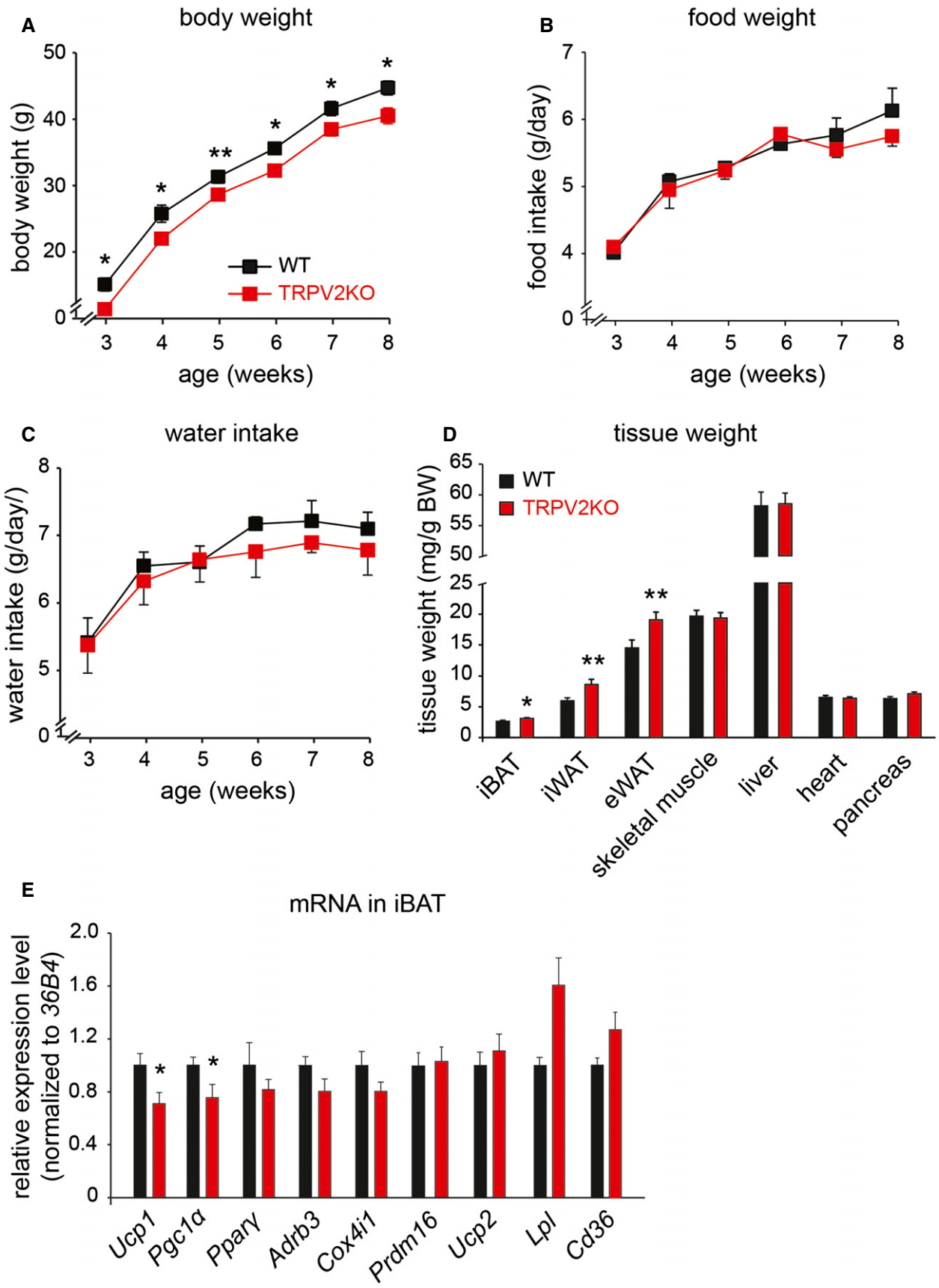

Figure 4.

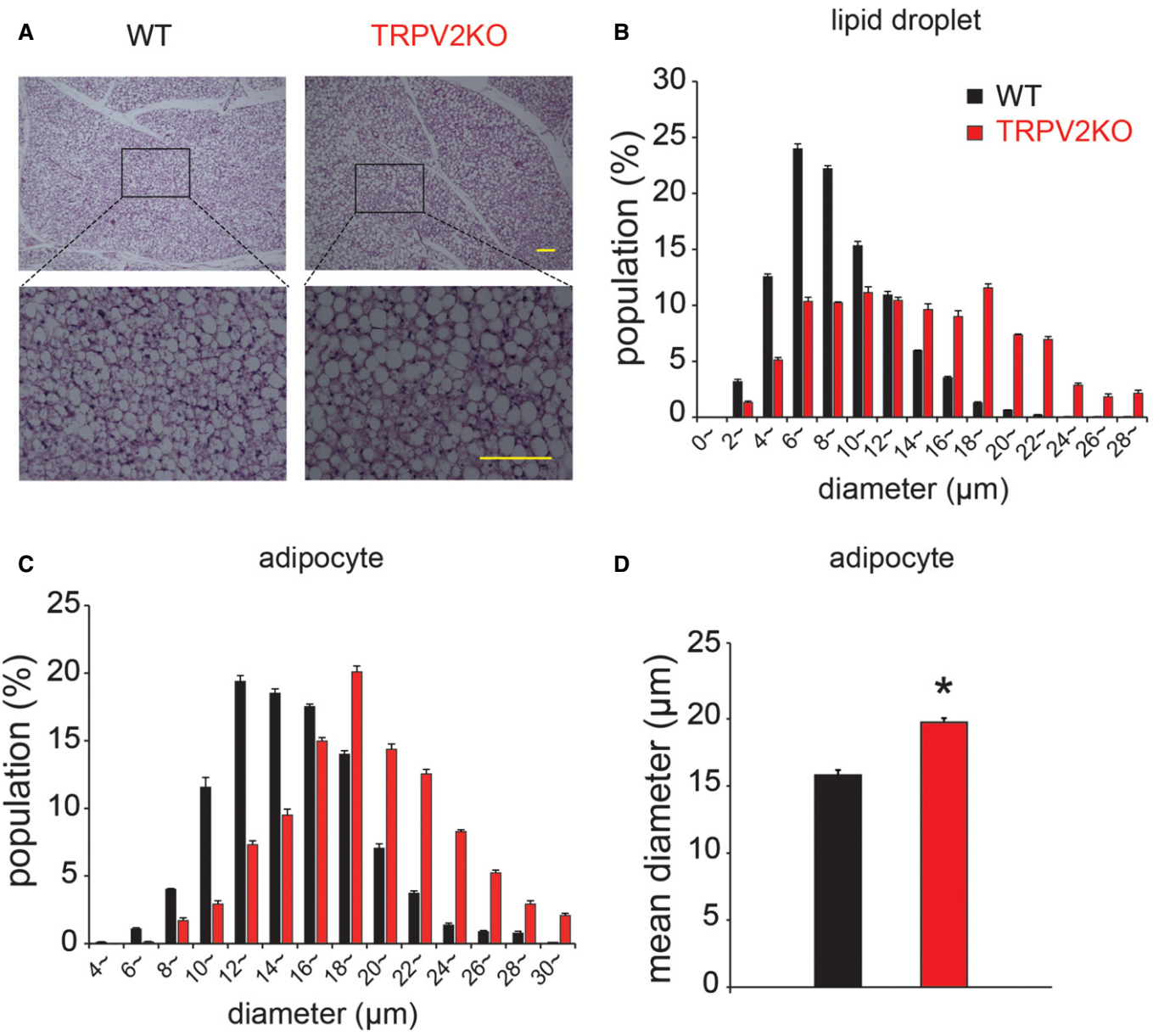

Figure 5. Comparison of adipocyte sizes between WT and TRPV2KO iBAT.

A Representative morphological results of iBAT by hematoxylin and eosin staining from 8-week-old WT and TRPV2KO mice. Scale bars indicate 100 μm.

B Comparison of lipid droplet size histograms from 8-week-old WT (black) and TRPV2KO (red) iBAT with hematoxylin and eosin staining. Mean values are 9.5 ± 0.2 μm in 8-week-old WT adipocytes, and 14.7 ± 0.2 μm in 8-week-old TRPV2KO adipocytes ($P < 0.01$). 1,000 to 1,400 droplets were counted. Data are presented as mean ± SEM, $n = 4$.

C Comparison of adipocyte size histograms from 8-week-old WT (black) and TRPV2KO (red) iBAT with hematoxylin and eosin staining. 800 to 1,000 cells were counted. Data are presented as mean ± SEM, $n = 4$.

D Mean diameters of adipocytes in 8-week-old WT mice (black) and TRPV2KO mice (red). Mean values are 15.8 ± 0.4 μm in 8-week-old WT adipocytes, and 19.8 ± 0.3 μm in 8-week-old TRPV2KO adipocytes. Data are presented as mean ± SEM, $n = 4$; *$P < 0.05$ vs. WT group. Unpaired Student's t-test.

iBAT (Fig EV2A), and histological analysis showed no difference in WT and TRPV2KO iWAT, either (Fig EV2B).

TRPV2KO mice exhibited cold intolerance

To address the involvement of TRPV2 in thermogenesis in iBAT, we analyzed TRPV2KO mice exposed to a cold environment. mRNA expression of *Ucp1* and *Pgc1a* was significantly increased upon exposure to cold stimulus at 4°C in WT iBAT, but the increases were small in TRPV2KO iBAT (Fig 6A and B), while mRNA level of *Pparg* was not changed upon cold exposure in these two genotypes (Fig 6C). Moreover, we found that *Trpv2* mRNA expression was significantly up-regulated in iBAT from WT mice upon cold exposure for 3 days (Fig 6D). Up-regulation of *Trpv2*

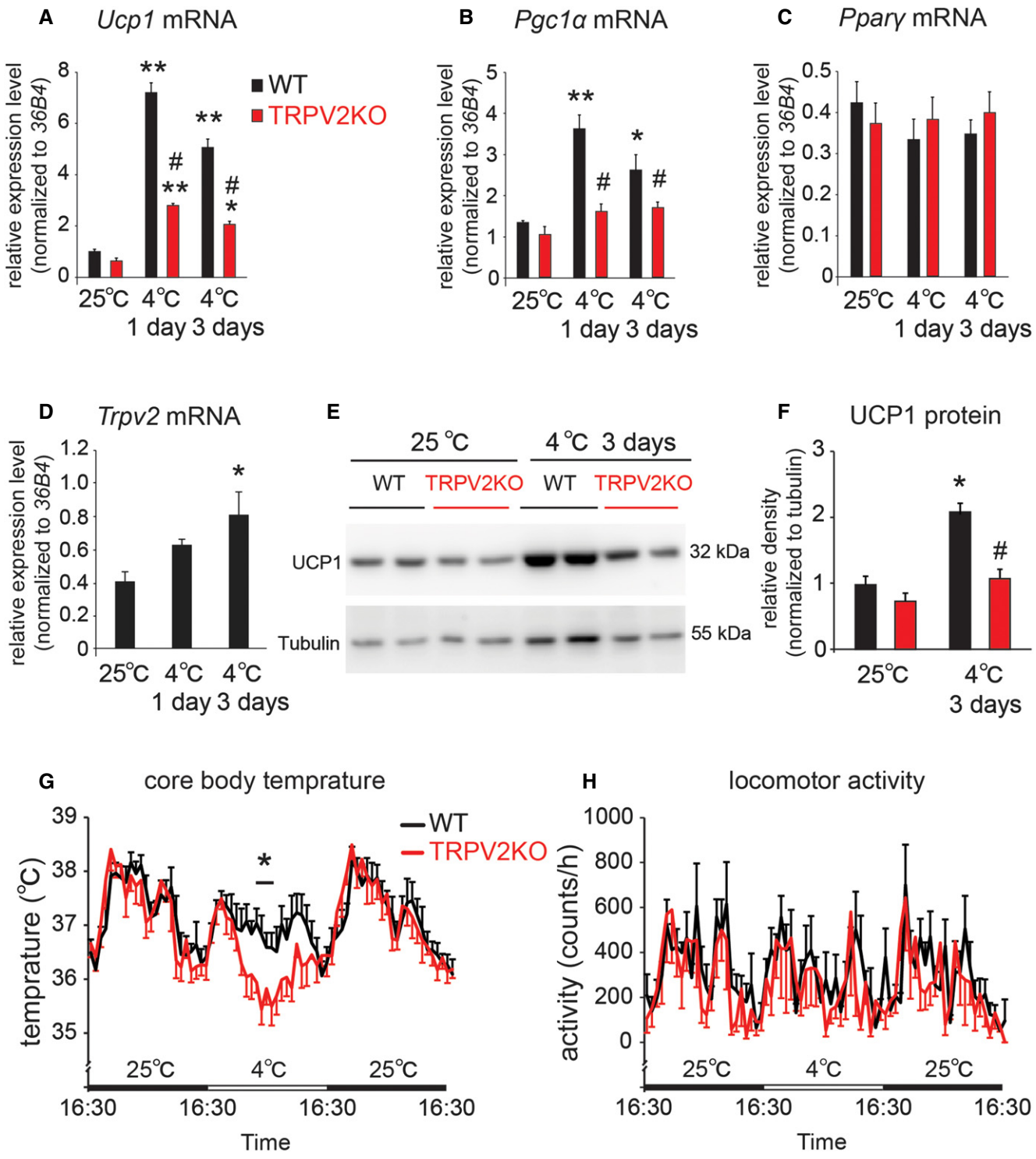

Figure 6. TRPV2KO mice show impaired cold-induced thermogenesis.

A–D Changes in mRNA expression of *Ucp1* (A), *Pgc1a* (B), *Pparg* (C), and *Trpv2* (D) in iBAT of WT and TRPV2KO mice before (25°C), after 1-day and 3-day cold (4°C) exposure. Mean ± SEM, n = 5–8; *$P < 0.05$; **$P < 0.01$ vs. 25°C group; $^{\#}P < 0.05$ vs. WT group. One-way ANOVA followed by 2-tailed t-test with Bonferroni correction.

E, F Western blot results of UCP1 protein in iBAT from WT and TRPV2KO mice before (25°C) and after 3-day cold (4°C) exposure (E). Comparison of UCP1 protein levels before and after cold exposure in iBAT from WT and TRPV2KO mice (F). Mean ± SEM, n = 6; *$P < 0.05$ vs. 25°C group; $^{\#}P < 0.05$ vs. WT group. One-way ANOVA followed by 2-tailed t-test with Bonferroni correction.

G, H Averages of core body temperatures (G) and activities (H) of WT and TRPV2KO mice with or without cold (4°C) exposure. Data are presented as mean ± SEM, n = 5; *$P < 0.05$ vs. WT group. Unpaired Student's t-test.

mRNA was also observed in iWAT upon cold exposure (Fig EV2C) which was accompanied by significant *Ucp1* increase, suggesting the iWAT "browning" (Fig EV2D). mRNA expression of *Ucp2* and *Lpl* was not different between WT and TRPV2KO iWAT (Fig EV2E). Increase in *Pgc1a* mRNA upon cold exposure was significantly smaller in TRPV2KO iWAT than in WT iWAT (Fig EV2G), while *Pparg* mRNA levels were not changed upon cold exposure in both WT and TRPV2KO iWAT (Fig EV2H). Increase in *Ucp1* mRNA upon cold exposure tended to be smaller in TRPV2KO iWAT, while no statistical significance was observed (Fig EV2F). These data suggested that TRPV2 plays some roles in iWAT similar to iBAT upon cold exposure. In addition, although an increase in UCP1 protein level was not observed in iBAT from WT mice exposed to a cold environment for 1 day (Fig EV3A and B), a significant increase in UCP1 protein was observed in iBAT from WT mice exposed to a cold environment for 3 days (Fig 6E and F). However, in iBAT from TRPV2KO mice, we did not observe cold exposure-induced induction of UCP1 protein after 3 days. Core body temperature and activity were not different between WT and TRPV2KO mice at a 25°C environment. Moreover, oxygen consumption in both dark and light periods did not differ between WT and TRPV2KO mice, either (Table 1). On the other hand, core body temperature was significantly decreased upon cold exposure in TRPV2KO mice without changes in activity (Fig 6G and H), suggesting that the basal level of energy expenditure was intact, while thermogenic function upon cold exposure was impaired in TRPV2KO mice.

β3-adrenergic receptor agonist-induced thermogenesis was impaired in TRPV2KO mice

To clarify the underlying mechanism of cold intolerance in TRPV2KO mice, we examined the thermogenic function of iBAT by intraperitoneal administration of a specific β3-adrenergic receptor agonist BRL37344. *Ucp1* and *Pgc1a* mRNA levels were significantly increased in WT iBAT by the BRL37344 administration, whereas the increases were significantly reduced in TRPV2KO iBAT (Fig 7A and B). *Pparg* mRNA levels were not increased in either WT or TRPV2KO iBAT (Fig 7C). Temperature increases in iBAT and the rectum in response to BRL37344 administration were significantly smaller in TRPV2KO iBAT than in WT iBAT (Fig 7D and E). Moreover, we did not observe any difference in iBAT NE turnover rates (Fig 7F) or rate constant k (Fig 7G) in WT and TRPV2KO mice upon cold stimulation. These results demonstrated that β3-adrenergic receptor stimulation-induced thermogenesis in BAT was impaired in TRPV2KO mice.

TRPV2KO mice showed severer obese phenotype after HFD treatment

Then, we asked whether TRPV2KO mice are prone to be obese when challenged with HFD because of the impaired thermogenesis in BAT. We treated both WT and TRPV2KO mice (13 week old) with HFD for 8 weeks continuously. Significant difference in body weight between WT and TRPV2KO mice (Fig 4A) was gone at an age of 10 weeks at a normal diet (Fig 8A). As expected, TRPV2KO mice showed significantly heavier body weight after starting a HFD treatment. Energy intake and water intake in TRPV2KO mice were also larger than in WT mice upon HFD (Fig EV3C and D). There was no significant difference in blood glucose levels (Fig 8B), while plasma insulin levels in TRPV2KO mice were significantly higher than in WT mice (Fig 8C). These results suggested that TRPV2KO mice showed insulin resistance. We also analyzed the weights of tissues related to energy metabolism in WT and TRPV2KO mice and found that weights of iBAT, iWAT, eWAT, and liver were significantly larger in TRPV2KO mice than in WT mice without significant difference in the weights of skeletal muscle (Fig 8D). Expression of *Ucp1* and *Pgc1a* mRNA in TRPV2KO iBAT was significantly lower than WT mice (Fig 8E) after 8-week HFD treatment, indicating that iBAT thermogenesis is significantly impaired in TRPV2KO mice even after HFD treatment. *Trpv2* mRNA was significantly up-regulated in both WT mice with HFD treatment (Fig EV4A) and db/db mice (Fig EV4B). These results revealed that TRPV2 is involved in the modulation of BAT thermogenesis under pathological conditions as well.

Discussion

In this study, we provided several lines of evidence that TRPV2 plays an important role in the maintenance of thermogenic function in BAT. We demonstrated that TRPV2 is functionally expressed in primary brown adipocytes. $[Ca^{2+}]_i$ changes possibly due to Ca^{2+} influx through TRPV2 are important for the induction of the thermogenic genes upon activation of sympathetic nervous system. Moreover, TRPV2KO mice exhibited cold intolerance and impaired BAT thermogenesis upon β3-adrenergic receptor activation. Most importantly, mice lacking TRPV2 are prone to be obese and insulin resistance upon fed with HFD. These findings demonstrate that TRPV2 activation in BAT could be an intriguing target for the treatment and prevention of human obesity and related metabolic diseases.

It is interesting that TRPV2 expression level was increased in the 6-day differentiated brown adipocytes. This increase also supports our findings that TRPV2 is involved in brown adipocyte differentiation (Fig 2B–D) and that TRPV2 is critical in the modulation of thermogenic gene expression (Fig 3B and C). However, transcription and translation mechanisms of TRPV2 are still unknown, while up-regulation of voltage-gated K^+ channels [33] and TRPM8 [28] was also observed during adipocyte differentiation. Genomewide binding analyses have revealed that many different genes were up-regulated during the differentiation of adipocytes through PPARγ and C/EBPα cooperation on multiple binding sites in their promoter regions [34,35]. Similar mechanisms might be involved in the TRPV2 up-regulation during adipocyte differentiation. It is reported that $[Ca^{2+}]_i$ increases stimulated by ionomycin inhibited white adipocyte differentiation [36]. In white adipocytes, either TRPV1 or TRPV3 activation-mediated Ca^{2+} influx prevents adipogenesis and plays anti-adipogenic roles *in vivo* [24,25]. In this study, we found that activation of TRPV2 by its ligands negatively regulated brown adipocyte differentiation. Furthermore, brown adipocytes lacking TRPV2 exhibited the facilitated differentiation. Thus, increase in $[Ca^{2+}]_i$ by TRPV2 activation might negatively regulate brown adipocyte differentiation *in vitro* as well.

TRPV2 could have a cell autonomous effect on the basal expression of thermogenic genes because the basal expression of

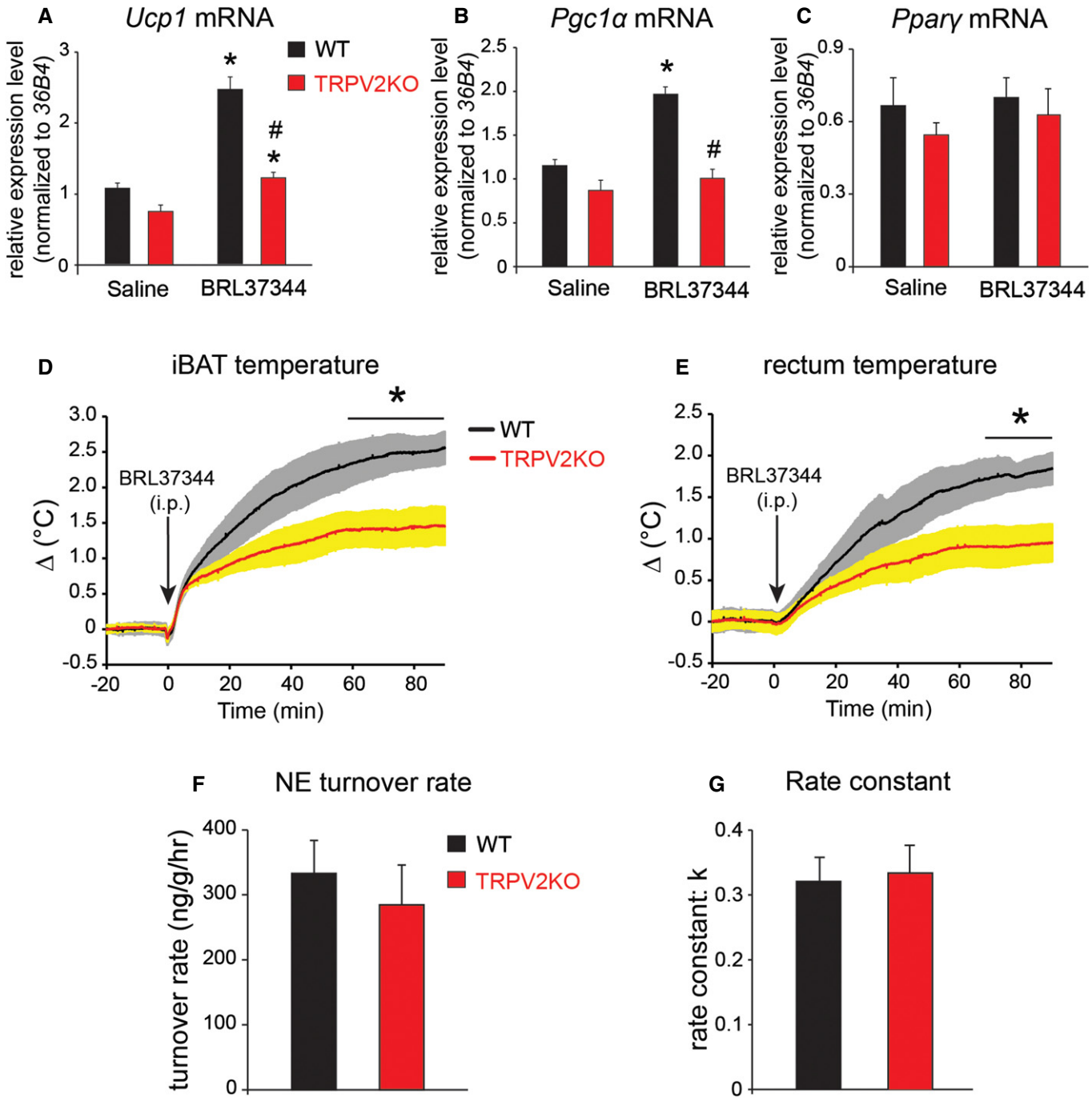

Figure 7. Comparison of thermogenic functions of iBAT in WT and TRPV2KO mice.

A–C Changes in mRNA expression of *Ucp1* (A), *Pgc1a* (B), and *Pparg* (C) from WT and TRPV2KO iBAT 4 h after intraperitoneal administration (i.p., arrows) of saline or a selective β3-adrenergic receptor agonist, BRL37344 (600 μg/kg body weight). Mean ± SEM, n = 5–7; *$P < 0.05$ vs. saline group; $^{\#}P < 0.01$ vs. WT BRL37344 administration group. One-way ANOVA followed by 2-tailed t-test with Bonferroni correction.

D, E Average traces of changes in iBAT temperature (D) or rectal body temperature (E) from WT and TRPV2KO mice after BRL37344 (600 μg/kg body weight) administration (i.p., arrows). Mean ± SEM, n = 5. *$P < 0.05$ vs. WT group. Unpaired Student's t-test.

F, G iBAT NE turnover rates (F) and rate constants k (G) in WT and TRPV2KO mice upon cold exposure (4°C) for 4 h. Data are presented as mean ± SEM, n = 8.

Ucp1 and *Pgc1a* was reduced in cultured TRPV2KO brown adipocytes (Fig 3A). Similar reductions in *Ucp1* and *Pgc1a* were observed in TRPV2KO iBAT (Fig 4E) although there is a possibility that gene expression was induced upon mild cold exposure at 25°C in mice not kept in the thermoneutral condition at around 29°C [37]. Alternatively, some ligands for TRPV2 exist both *in vitro* and *in vivo*. Candidate TRPV2 stimuli include mechanical stimulation (membrane stretch), LPC, LPI, and endocannabinoids

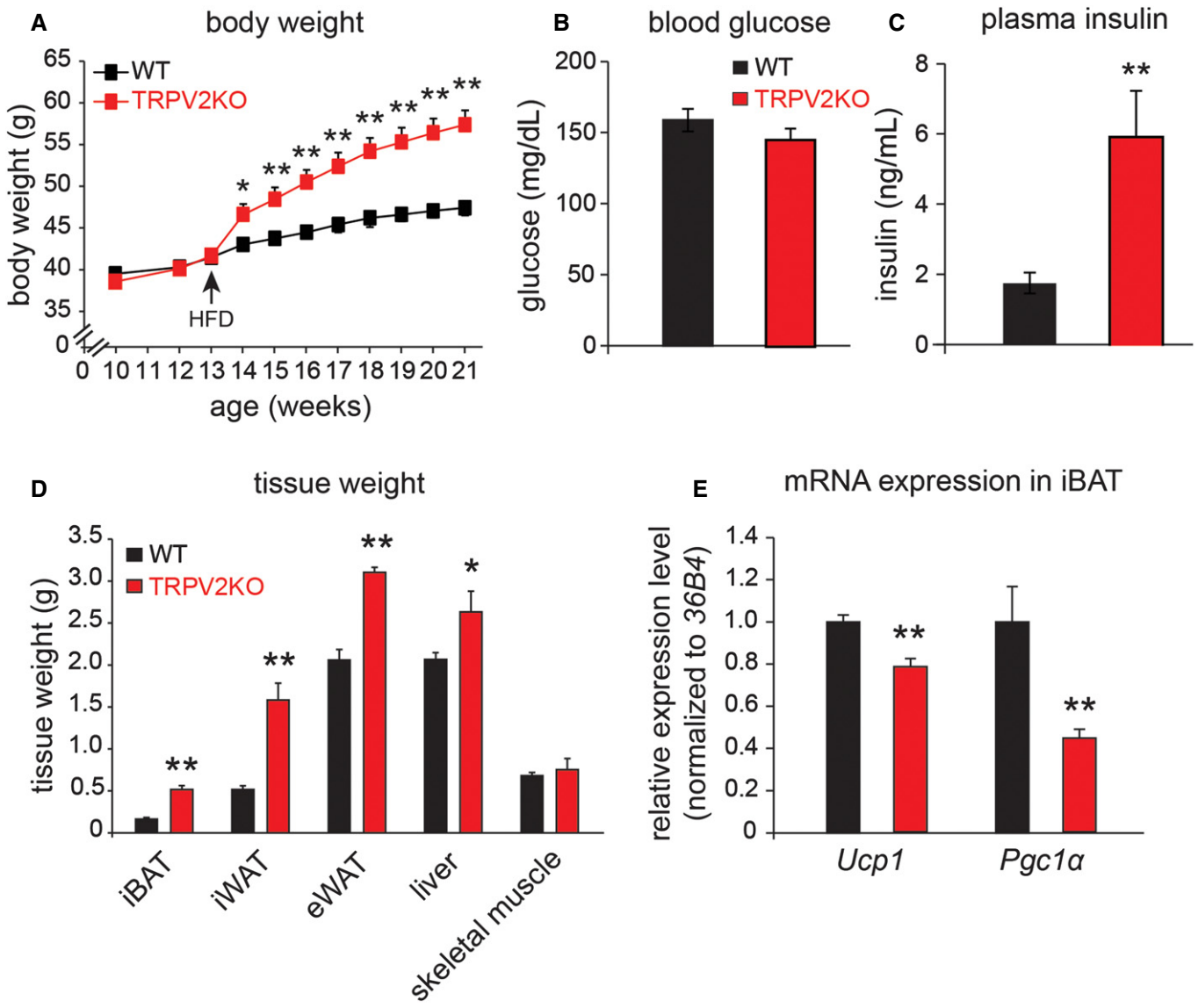

Figure 8. Comparison of the changes upon high-fat-diet treatment between WT and TRPV2KO mice.

A Body weight changes between WT and TRPV2KO mice treated with high-fat diet (HFD) for 8 weeks continuously from 13 weeks of age.

B, C Blood glucose level (B) and plasma insulin level (C) of WT and TRPV2KO mice after 8-week HFD treatment.

D Weights of tissues related to energy metabolism in WT and TRPV2KO mice after 8-week HFD treatment.

E mRNA expression of *Ucp1* and *Pgc1a* in iBAT from WT and TRPV2KO mice after 8-week HFD treatment.

Data information: All data are presented as mean ± SEM, WT mice ($n = 6$), TRPV2KO mice ($n = 8$); $^*P < 0.05$; $^{**}P < 0.01$ vs. WT group. Unpaired Student's *t*-test.

[19,21,22,38]. Moreover, IGF-1 is known to enhance transient translocation of TRPV2 from intracellular compartments to the plasma membrane through a PI3K-dependent pathway [39,40]. In that case, an increase in TRPV2 incorporation into the plasma membrane could be sufficient for TRPV2 activation due to membrane stretch. In addition, our data suggest a possibility that TRPV2 activation is involved in β3-adrenergic receptor-mediated thermogenesis without changes in β3-adrenergic receptor expression.

In addition to the *in vitro* analysis, *in vivo* studies demonstrate that the absence of TRPV2 led to down-regulation of thermogenic genes (Fig 4E), enlarged sizes of brown adipocytes in iBAT (Fig 5), and impaired BAT thermogenesis in response to cold stimulus (Fig 6). Similar iBAT abnormalities were reported in aged and obese mice [41,42]. It has also been reported that UCP1 knockout mice show accumulated lipid droplets in brown adipocytes and consume less oxygen upon treatment with a β3-adrenergic receptor agonist [43]. Taken together, we conclude that TRPV2KO mice exhibited impairments in iBAT thermogenesis. However, basal blood glucose levels, plasma insulin levels, lipid metabolism parameters, and oxygen consumption in both dark and light periods showed no differences between these two genotypes (Table 1). These data indicate that impairment of iBAT function in TRPV2KO mice is not sufficient to cause the changes

in above parameters in the basal condition and that TRPV2 is critical for iBAT thermogenesis in the specific conditions such as cold environment. Meanwhile, we cannot exclude the involvement of TRPV2 expressed in other tissues [32,44] although NE utilization was normal in TRPV2KO mice (Fig 7F and G) and contribution of TRPV2 in BAT macrophages did not look great (Fig EV1). Nevertheless, the fact that similar difference in gene expression and temperature increases between WT and TRPV2KO mice were observed not only in response to cold exposure (Fig 6) but also to administration of a β3-adrenergic receptor agonist (Fig 7) indicates that TRPV2 in iBAT is critical for adaptive thermogenesis.

TRPV2KO mice are prone to be obese and showed insulin resistance after HFD treatment (Fig 8A). These findings further support our conclusion that the impaired thermogenesis has occurred in BAT lacking TRPV2. It has been reported that several TRP knockout mice are resistant to HFD-induced obesity [29,45–47], an opposite phenotype observed in TRPV2KO mice. Our results suggest that activation of TRPV2 could be an intriguing therapeutic approach for the treatment and prevention of human obesity. And specific TRPV2 agonists are necessary to be developed. Insulin resistance observed upon a HFD treatment suggests that other tissues could be also involved in the severe obese phenotype of TRPV2KO mice since TRPV2 has been reported to be expressed in many cell types such as pancreatic β-cells [48]. Up-regulation of *Trpv2* in obese mice also indicates the involvement of TRPV2 in iBAT thermogenesis under pathological conditions (Fig EV4A and B). Moreover, the increase in *Trpv2* in iWAT of WT mice (Fig EV2C) and the impaired induction of *Pgc1a* in iWAT of TRPV2KO mice upon cold exposure (Fig EV2G) suggest that TRPV2 could play a relevant role in white adipocytes and might be involved in iWAT "browning" *in vivo* as well. Taken together, our results suggest that the importance of TRPV2 in iBAT thermogenesis contributes to the obese phenotype in TRPV2KO mice fed with HFD.

It is still unclear how TRPV2 activation modulates energy expenditure. There is one study in which slow $[Ca^{2+}]_i$ increases were observed upon β3-adrenergic receptor stimulation in brown adipocytes [49]. It has also been reported that TRPM8 stimulation by its ligands increased UCP1 expression in brown adipocytes and BAT through PKA phosphorylation [26]. Moreover, in white adipocytes, activation of TRPV1 by capsaicin or TRPM8 by cold temperature or menthol enhanced UCP1 expression [27,28]. On the other hand, ERK1/2 were reported to be activated by TRPV4 signaling [50], and TRPV4 activation caused a rapid phosphorylation of ERK1/2 and JNK1/2, which further suppressed the mRNA levels of *Ucp1* and *Pgc1a* [29]. A TRPV1 agonist, capsaicin prevented adipogenesis in both *in vitro* and *in vivo* conditions [24], which is probably through the calcineurin pathway [51]. TRPV3 activation inhibited the expression of adipogenic genes, PPARγ and C/EBPα via a PI3K/Akt/FOXO1 pathway, which further suppressed the adipogenesis of white adipocyte *in vitro* and WAT *in vivo* [25]. In this study, lack of TRPV2 suppressed the mRNA levels of *Ucp1* and *Pgc1a* in brown adipocytes and impaired BAT thermogenic function without changes in the expression of *Trpv1*, *Trpv3*, or *Trpv4* (Fig EV4C). Since TRPV2 is a non-selective Ca^{2+}-permeable cation channel, activation of TRPV2 leads to $[Ca^{2+}]_i$ increases (Figs 1E and EV1E–G), indicating that $[Ca^{2+}]_i$ changes could be involved in the differentiation and thermogenic gene induction upon β-adrenergic receptor activation. Indeed, BAPTA-AM significantly suppressed the increased expression of thermogenic genes, *Ucp1* and *Pgc1a* inducted by ISO (Fig 3F and G). Therefore, $[Ca^{2+}]_i$ increases possibly through Ca^{2+}-permeable TRP channels could be important for the adipocyte functions. And high mRNA expression of *Trpv2* in BAT suggests that regulation of Ca^{2+} influx by TRPV2 is critical for BAT functions. Because adipocytes play a lot of pivotal functions, multiple Ca^{2+} influx pathways could exist although we still do not know the mechanisms of apparent opposite functions between TRPV4 and others. It would be intriguing to examine which pathways described above are involved in the $[Ca^{2+}]_i$ increases downstream of TRPV2 activation.

In conclusion, our study clearly established a role for TRPV2-mediated Ca^{2+} influx in the thermogenic function and differentiation of BAT. With the recent reports that BAT is present in adult humans [6], approaches modulating BAT function through TRPV2 could be intriguing ways to treat human obesity and related metabolic disorders although there have been no reports of the expression of TRPV2 in human brown adipocyte cell line or human brown adipose tissues.

Materials and Methods

Animals

Male C57Bl/6NCr mice (SLC, Hamamatsu, Japan) were housed in a controlled environment (12-h light/dark cycle; 22–24°C; 50–60% humidity) with food and water *ad libitum*. For all *in vivo* experiments, 8- to 13-week-old wild-type (WT) and TRPV2KO male mice were individually housed in controlled environmental chambers (Nihon Medical and Chemical Instruments) in which temperature is easily manipulated. For HFD treatment experiments, WT or TRPV2KO mice were fed with HFD (40% fat by calories; CLEA Rodent Diet Quick Fat, Japan) *ad libitum* for 6–12 weeks. BKS.Cg-Dock7^{m}+/+Lepr^{db}/J (db/db mice) and BKS.Cg-Dock7^{m}+/+Lepr$^{db/+}$/J (control mice) were purchased from Charles River (Yokohama, Japan). All animal protocols were approved by the Animal Research Committee, National Institute for Physiological Sciences of Japan (Okazaki, Japan), and were performed in accordance with institutional guidelines. We made a randomization in the *in vivo* analyses and did the experiments in the blinding manner.

Generation of TRPV2KO mice

Construction of the targeted allele, establishment of targeted embryonic stem (ES) cells, and generation of the chimera and F1 mice were carried out by Unitech Co. (Chiba, Japan). Briefly, the exons 3–5 of mouse *Trpv2* were flanked by two loxP sequences (Fig EV5A). An Flp recognition target (FRT)-flanked neo-cassette was inserted upstream of exon 3. The targeting vector was electroporated into C57BL/6 mouse ES cells. Positive clones were selected, and homologous recombination was confirmed by Southern blotting (Fig EV5B). The targeted ES cells were injected into blastocysts (BALB/c), and then, chimera mice were bred with C57BL/6 mice to generate founder mice. The founder mice were crossed with the FLPe deleter mice, producing heterozygous flox mice without the neo-cassette (*TRPV2*$^{lox/+}$). The heterozygous

flox mice were intercrossed to obtain homozygous flox mice ($TRPV2^{lox/lox}$). Genotyping was performed using PCR (Fig EV5C). PCR primers for genotyping were as follows: forward primer, 5′-GTCTCACTGAACTCTGCTAGACTGG-3′ on the short arm, reverse primer 1, 5′-ATAGCCTGGGATACTCTGTCTCAAG-3′ on exon 3, yielding PCR products of 248 bp (WT allele) and 432 bp (targeted allele), and reverse primer 2, 5′-GTGATAACCACAGCAGAACA TAGTG-3′ on the long arm, confirming successful *Cre* recombination. After *Cre*-mediated recombination, all of TRPV2 channel structure and detectable protein were ablated. To overcome prenatal lethality observed in TRPV2KO mice on a C57Bl/6NCr background, we generated WT and $TRPV2^{+/-}$ F3 hybrids by crossing C57Bl/6NCr $TRPV2^{+/-}$ mice with ICR WT mice, and then, $TRPV2^{+/-}$ F3 hybrids were mated to each other to generate F3 hybrids TRPV2KO mice. The resulting TRPV2KO mice appeared as healthy as WT mice. WT mice with the same background were also obtained by crossing $TRPV2^{+/-}$ F3 hybrids.

Primary culture of mouse brown adipocytes

Primary culture of mouse brown adipocytes was done according to previously reported methods with slight modification [52]. In brief, pre-adipocytes were isolated from iBAT of six male mice (3 week old). After getting confluent, pre-adipocytes were inducted in standard medium supplemented with 500 μmol/l 3-isobutyl-1-methylxanthine and 1 μmol/l dexamethasone (induction medium) at the standard incubation condition for 2 days, and then, cells were differentiated in standard medium supplemented with 50 nmol/l triiodothyronine (T3) and 17.4 mmol/l insulin (differentiation medium) for 6 more days. For the pharmacological studies in the thermogenesis experiments, compounds were applied in differentiation medium after 6 days of differentiation. To check the involvement of TRPV2 in brown adipocyte differentiation, we used two kinds of medium with different concentrations of T3 and insulin: the same as above differentiation medium (control) and ten-time-diluted medium containing 5 nmol/l T3 and 1.74 mmol/l insulin (1/10 suppl.). TRPV2 agonists were applied when medium was changed from the induction medium to the differentiation medium for 6 consecutive days to induce differentiation.

Isolation of adipose tissue macrophages from iBAT

Brown adipocytes and stromal vascular fractions (SVFs) were isolated from 5 WT mice (8 week old) iBAT by collagenase digestion and mechanical shaking following a method previously reported with a few modifications [53]. Cell suspensions of SVFs were further divided using a magnetic cell sorting system (Miltenyi Biotec, Auburn, CA, USA) to obtain CD11b-positive cells (macrophages, CD11b (+) cells) following the manufacturer's instructions. Isolated adipocytes, CD11b-negative cells, and macrophages from iBAT were used for further experiments.

RT–PCR

Total RNA was isolated using Sepasol-RNA I Super G (Nacalai Tesque Inc., Kyoto, Japan) according to the manufacturer's protocol. In brief, mouse tissues or cells were freshly collected and homogenized in Sepasol-RNA I Super G on ice. RT–PCR was performed using the SuperScript® III kit (Invitrogen, Carlsbad, CA, USA). The RNA was digested with RNase H at 37°C for 20 min. The primer sequence information is summarized in Table EV1.

Quantitative real-time RT–PCR

Copy numbers of mouse genes were determined by quantitative RT–PCR (qRT–PCR) using SYBR Green MASTER (Invitrogen, Carlsbad, CA, USA) following the manufacturer's protocol. Data were collected during each extension phase of the PCR and analyzed using ABI-7700 SDS software (Applied Biosystems, Foster City, CA, USA). The results were standardized for comparison by measuring levels of *36B4* mRNA in each sample. The primer sequence information is shown in Table EV2.

Immunoprecipitation and Western blotting

Brown adipocytes were collected and lysed in 100 μl RIPA lysis buffer with complete protease inhibitor cocktail (Roche Molecular Biochemicals, Basel, Switzerland). HEK293 cells transfected with *mTrpv2* plasmid DNA were used for the positive control. Cells were lysed in 100 μl RIPA lysis buffer with protease inhibitor cocktail. Cell lysates were pre-cleared with protein G Sepharose beads (GE Healthcare, Buckinghamshire, UK) with rotation at 4°C for 2 h. The supernatants were collected after centrifugation and incubated with anti-TRPV2 antibody (TransGenic, Kobe, Japan) at 4°C overnight, and precipitated with protein G Sepharose beads (GE Healthcare) for 2 h in Micro Bio-Spin Chromatography Columns (Bio-Rad, Munich, Germany). The samples were denaturized at 95°C for 5 min and separated on an 8% SDS–PAGE gel and transferred onto a PVDF membrane. The membrane was blocked using BlockAce reagent (Snow Brand Milk Products Co., Tokyo, Japan) at 4°C overnight and then incubated with an anti-TRPV2 antibody or anti-tubulin monoclonal antibody diluted 1:1,000 at room temperature for 1 h. After three washes with PBS-T (0.1% Triton X-100), the membrane was incubated at room temperature for 1 h with an anti-rabbit IgG or anti-mouse IgG HRP-linked antibody (Cell Signaling Technology, Boston, MA, USA) diluted 1:5,000. The signals were visualized with an ECL kit (Pierce, IL, USA), and the PVDF membrane was photographed using a LAS-3000 imaging system (Fujifilm, Tokyo, Japan).

Ca^{2+}-imaging

Intracellular Ca^{2+} concentration was monitored by loading primary cultured brown adipocytes with Fura-2 AM fluorescent dye (Invitrogen, Carlsbad, CA, USA). Adipocytes were incubated with 5 μmol/l Fura-2 AM for 30 min and used in experiments within 3 h. Fluorescent signals were collected with a CCD camera (Hamamatsu Photonics, Hamamatsu, Japan) and recorded by IP Lab software (Scanalytics, Inc., Rockville, MD, USA) at three-second intervals. The bath solution contained 140 mmol/l NaCl, 5 mmol/l KCl, 2 mmol/l $MgCl_2$, 2 mmol/l $CaCl_2$, 10 mmol/l HEPES, and 10 mmol/l glucose, pH 7.4, adjusted with NaOH. A positive response was obtained when the 340/380 ratio increased more than 0.2 evoked by 2APB or LPC. Norepinephrine responses indicated

cells were differentiated brown adipocytes. Cell viability was confirmed with 5 μmol/l ionomycin. All the experiments were performed at room temperature.

Electrophysiology

For whole-cell patch-clamp recording experiments, 6-day differentiated mouse brown adipocytes were used. The bath solution was the same as that used for Ca^{2+} imaging. The pipette solution contained 140 mmol/l KCl, 5 mmol/l EGTA, and 10 mmol/l HEPES, pH 7.4, adjusted with KOH. Data were sampled at 10 kHz and filtered at 5 kHz using an Axopatch 200B amplifier (Axon Instruments, Sunnyvale, CA, USA). The membrane potential was clamped at −60 mV during the whole-cell patch-clamp recordings, and voltage-ramp pulses from −100 mV to + 100 mV for 300 ms were applied in a 5-s period. All patch-clamp experiments were performed at room temperature. Data were analyzed using pCLAMP10.4 software (Axon Instruments, Sunnyvale, CA, USA).

Oil red O staining and triglyceride level measurement of brown adipocytes

Oil red O staining was performed using oil red O dye (Sigma, St. Louis, USA). In brief, the adipocytes were fixed with 4% formalin and incubated at room temperature for at least 1 h. After fixation, cells were washed with purified water twice and washed with 60% isopropanol at room temperature for 5 min. The cells were let dried completely at room temperature, and oil red O solution was added and then incubated at room temperature for 10 min. Oil red O solution was removed with addition of purified water immediately, and the cells were washed 4 times with purified water. Images were acquired under the microscope (Olympus, Tokyo, Japan) for analysis. For the measurement of triglyceride levels, all the water was removed and cells were dried completely. Oil red O dye was eluted with 100% isopropanol and incubated with gently shaking for 10 min. The OD values were measured at 490 nm using a multiscan spectrum (Thermo Scientific, Waltham, MA, USA) with 100% isopropanol as a blank.

The number of differentiated brown adipocytes counting

Differentiated brown adipocytes were counted in the pictures taken under the microscope. At least six random fields were chosen in each dish. Adipocytes could be distinguished from pre-adipocytes by the presence of visible lipid droplets. For better visualization, lipids were stained with oil red O and only cells positive for this stain were considered as differentiated adipocytes.

Histological analysis

Eight-week-old WT and TRPV2KO male mice with the same background were used. iBAT and iWAT tissues were fixed in 4% paraformaldehyde/PBS, embedded in paraffin wax, and sectioned at 8 μm. iBAT sections were then de-paraffinized in xylene. The sections were stained in hematoxylin solution for 5 min and eosin solution for 10 min. Then, the sections were immersed in decreasing ethanol solutions from 100% to 70% following a dehydration process. The sections were finally penetrated with xylene for 5 min, 3 times, mounted, and observed by light microscopy (Keyence, Tokyo, Japan). Adipocyte sizes were assessed by measuring the diameter of lipid droplets and adipocyte sizes using ImageJ software (National Institutes of Health, Bethesda, MD, USA).

Blood biochemical measurements

Blood glucose levels were measured using a glucose monitor (Arkray, Kyoto, Japan), and plasma insulin levels were examined using ELISA (Morinaga Institute of Biological Science, Inc., Yokohama, Japan). Total cholesterol and non-esterified fatty acid (NEFA) levels were measured using commercial kits following instructions from the manufacturer (WAKO Pure Chemical Industries, Ltd., Osaka, Japan).

Measurement of oxygen consumption

The oxygen consumption was measured using an indirect calorimetric system (Oxymax Equal Flow 8 Chamber/Small Subject System; Columbus Instruments, Columbus, OH, USA) equipped with an eight-chamber airtight metabolic cage at room temperature. The data for each chamber were collected every 9 min, with room air as a reference, and measured for 20 h from 9 PM to 5 PM.

Body temperature measurement of freely behaving mice

Core body temperature and activities were monitored using transmitter devices (TA-F10 Mouse Temperature Transmitter, DSI Company, St. Paul, USA) surgically implanted in the peritoneal cavity under anesthesia (2.0% isoflurane in 100% O_2 through a tracheal cannula with the animal's spontaneous ventilation). After surgery, each animal was housed alone in a cage and allowed to recover from surgery for more than 1 week. Data were recorded by placing each cage containing an animal implanted with a radiotransmitter on a receiver plate (DSI PhysioTel® Receivers—RPC-1, DSI Company). A Vital View Data Acquisition System (Dataquest ART, DSI Company) was used for data collection and analysis. After cold exposure, iBAT was dissected and collected immediately for the designated experiments.

In vivo iBAT temperature recording

Eight-week-old mice were anesthetized with 2.0% isoflurane in 100% O_2 through a tracheal cannula with the animal's spontaneous ventilation. Each mouse was fixed on an electric heating pad to keep core body temperature within the range of 37–37.5°C. Thermoprobes (Unique Medical, Japan) were inserted into the iBAT tissue and the rectum. Recordings were started 20 min after the signals became stable. BRL37344 (600 μg/kg body weight) was administrated by intraperitoneally. Spike 2 software was used to obtain a continuous measurement of iBAT, rectal, and ambient temperatures.

iBAT norepinephrine measurement and calculation

Twenty-four mice were handled carefully for 7 days at the same time point (11 AM) of the day. Mice were divided into 4 groups.

The experiment started at 11 AM, and the concentrations of norepinephrine (NE) in iBAT following intraperitoneal injection of α-methyl-L-tyrosine (AMPT) 300 mg/kg 4 h without (25°C) or with cold exposure (4°C) were measured. After cold exposure, iBAT was rapidly dissected, weighed, and frozen in nitrogen to measure NE concentrations. For measurement of NE concentrations, dihydroxybenzylamine hydrobromide was added as an internal standard, and the tissue was homogenized in 1 ml of 0.4 mol/l perchloric acid (PCA). After centrifugation, the NE in the supernatant was purified with activated alumina, as described previously [54]. Then, tissue NE was eluted with 100 μl of 0.4 mol/l PCA. NE was assayed by high-performance liquid chromatography with electrochemical detection [55]. The detector potential was set at 700 mV maintained across a glassy carbon working electrode. Methanol buffer (10:90, v/v) composed of 50 mmol/l potassium phosphate buffer (pH 3.5), 10 μmol/l EDTA·2Na, and 100 mg/l sodium 1-octanesulfonate was used as the mobile phase at a flow rate of 1 ml/min. The NE turnover rates and rate constants were calculated as previously reported [56].

Statistical analysis

Group data are presented as the mean ± SEM. Statistical analysis was performed with Student's *t*-test or one-way ANOVA followed by multiple *t*-tests with Bonferroni correction using Origin 8.5 software. Only two-tailed *P*-values < 0.05 were considered to represent a significant difference.

Expanded View for this article is available online.

Acknowledgements
We are grateful to Dr. Yasuhiko Minokoshi and Dr. Kazuhiro Ikenaka (National Institute for Physiological Sciences) and Dr. Toshihiko Yada from Jichi Medical University for their kind discussions. We also thank Ms. Keiko Fukuoka for her technical help. This work was supported by grants from the Japanese Ministry of Education, Culture, Sports, Science and Technology (#23249012 for M.T., #24111561 for K.U.), and Takeda Science Foundation (K.U.).

Author contributions
WS, KU, and MT designed experiments and wrote the manuscript. WS performed experiments. WS, KU, YS, YZ, MK, YT, NT, TG, TK, and MT discussed and interpreted the data. KU, YS, YZ, MK, YT, NT, and TG gave technique assistances. SW and YI supplied TRPV2KO mice. KU and MT supervised this work.

Conflict of interest
The authors declare that they have no conflict of interest.

References

1. Ahn J, Lee H, Kim S, Park J, Ha T (2008) The anti-obesity effect of quercetin is mediated by the AMPK and MAPK signaling pathways. *Biochem Biophys Res Commun* 373: 545 – 549
2. Pi-Sunyer FX (2002) The obesity epidemic: pathophysiology and consequences of obesity. *Obes Res* 10(Suppl 2): 97S – 104S
3. Hajer GR, van Haeften TW, Visseren FL (2008) Adipose tissue dysfunction in obesity, diabetes, and vascular diseases. *Eur Heart J* 29: 2959 – 2971
4. Argyropoulos G (1985) Harper ME (2002) Uncoupling proteins and thermoregulation. *J Appl Physiol* 92: 2187 – 2198
5. Mozo J, Emre Y, Bouillaud F, Ricquier D, Criscuolo F (2005) Thermoregulation: what role for UCPs in mammals and birds? *Biosci Rep* 25: 227 – 249
6. Cypess AM, Lehman S, Williams G, Tal I, Rodman D, Goldfine AB, Kuo FC, Palmer EL, Tseng YH, Doria A *et al* (2009) Identification and importance of brown adipose tissue in adult humans. *N Engl J Med* 360: 1509 – 1517
7. van Marken Lichtenbelt WD, Vanhommerig JW, Smulders NM, Drossaerts JM, Kemerink GJ, Bouvy ND, Schrauwen P, Teule GJ (2009) Cold-activated brown adipose tissue in healthy men. *N Engl J Med* 360: 1500 – 1508
8. Nedergaard J, Cannon B (2010) The changed metabolic world with human brown adipose tissue: therapeutic visions. *Cell Metab* 11: 268 – 272
9. Nedergaard J, Bengtsson T, Cannon B (2011) New powers of brown fat: fighting the metabolic syndrome. *Cell Metab* 13: 238 – 240
10. Ghorbani M, Himms-Hagen J (1997) Appearance of brown adipocytes in white adipose tissue during CL 316,243-induced reversal of obesity and diabetes in Zucker fa/fa rats. *Int J Obes Relat Metab Disord* 21: 465 – 475
11. Guerra C, Koza RA, Yamashita H, Walsh K, Kozak LP (1998) Emergence of brown adipocytes in white fat in mice is under genetic control. Effects on body weight and adiposity. *J Clin Invest* 102: 412 – 420
12. Nedergaard J, Ricquier D, Kozak LP (2005) Uncoupling proteins: current status and therapeutic prospects. *EMBO Rep* 6: 917 – 921
13. Feldmann HM, Golozoubova V, Cannon B, Nedergaard J (2009) UCP1 ablation induces obesity and abolishes diet-induced thermogenesis in mice exempt from thermal stress by living at thermoneutrality. *Cell Metab* 9: 203 – 209
14. Wang Q, Zhang M, Ning G, Gu W, Su T, Xu M, Li B, Wang W (2011) Brown adipose tissue in humans is activated by elevated plasma catecholamines levels and is inversely related to central obesity. *PLoS ONE* 6: e21006
15. Berridge MJ, Bootman MD, Roderick HL (2003) Calcium signalling: dynamics, homeostasis and remodelling. *Nat Rev Mol Cell Biol* 4: 517 – 529
16. Worrall DS, Olefsky JM (2002) The effects of intracellular calcium depletion on insulin signaling in 3T3-L1 adipocytes. *Mol Endocrinol* 16: 378 – 389
17. Caterina MJ, Rosen TA, Tominaga M, Brake AJ, Julius D (1999) A capsaicin-receptor homologue with a high threshold for noxious heat. *Nature* 398: 436 – 441
18. Juvin V, Penna A, Chemin J, Lin YL, Rassendren FA (2007) Pharmacological characterization and molecular determinants of the activation of transient receptor potential V2 channel orthologs by 2-aminoethoxydiphenyl borate. *Mol Pharmacol* 72: 1258 – 1268
19. Monet M, Gkika D, Lehen'kyi V, Pourtier A, Vanden Abeele F, Bidaux G, Juvin V, Rassendren F, Humez S, Prevarsakaya N (2009) Lysophospholipids stimulate prostate cancer cell migration via TRPV2 channel activation. *Biochim Biophys Acta* 1793: 528 – 539
20. Ramsey IS, Delling M, Clapham DE (2006) An introduction to TRP channels. *Annu Rev Physiol* 68: 619 – 647
21. Muraki K, Iwata Y, Katanosaka Y, Ito T, Ohya S, Shigekawa M, Imaizumi Y (2003) TRPV2 is a component of osmotically sensitive cation channels in murine aortic myocytes. *Circ Res* 93: 829 – 838
22. Iwata Y, Katanosaka Y, Arai Y, Shigekawa M, Wakabayashi S (2009) Dominant-negative inhibition of Ca2+ influx via TRPV2 ameliorates muscular dystrophy in animal models. *Hum Mol Genet* 18: 824 – 834
23. Lee E, Jung DY, Kim JH, Patel PR, Hu X, Lee Y, Azuma Y, Wang HF, Tsitsilianos N, Shafiq U *et al* (2015) Transient receptor potential vanilloid

type-1 channel regulates diet-induced obesity, insulin resistance, and leptin resistance. *FASEB J* 29: 3182 – 3192

24. Zhang LL, Yan Liu D, Ma LQ, Luo ZD, Cao TB, Zhong J, Yan ZC, Wang LJ, Zhao ZG, Zhu SJ *et al* (2007) Activation of transient receptor potential vanilloid type-1 channel prevents adipogenesis and obesity. *Circ Res* 100: 1063 – 1070
25. Cheung SY, Huang Y, Kwan HY, Chung HY, Yao X (2015) Activation of transient receptor potential vanilloid 3 channel suppresses adipogenesis. *Endocrinology* 156: 2074 – 2086
26. Ma S, Yu H, Zhao Z, Luo Z, Chen J, Ni Y, Jin R, Ma L, Wang P, Zhu Z *et al* (2012) Activation of the cold-sensing TRPM8 channel triggers UCP1-dependent thermogenesis and prevents obesity. *J Mol Cell Biol* 4: 88 – 96
27. Baboota RK, Singh DP, Sarma SM, Kaur J, Sandhir R, Boparai RK, Kondepudi KK, Bishnoi M (2014) Capsaicin induces "brite" phenotype in differentiating 3T3-L1 preadipocytes. *PLoS ONE* 9: e103093
28. Rossato M, Granzotto M, Macchi V, Porzionato A, Petrelli L, Calcagno A, Vencato J, De Stefani D, Silvestrin V, Rizzuto R *et al* (2014) Human white adipocytes express the cold receptor TRPM8 which activation induces UCP1 expression, mitochondrial activation and heat production. *Mol Cell Endocrinol* 383: 137 – 146
29. Ye L, Kleiner S, Wu J, Sah R, Gupta RK, Banks AS, Cohen P, Khandekar MJ, Bostrom P, Mepani RJ *et al* (2012) TRPV4 is a regulator of adipose oxidative metabolism, inflammation, and energy homeostasis. *Cell* 151: 96 – 110
30. Lowell BB, Flier JS (1997) Brown adipose tissue, beta 3-adrenergic receptors, and obesity. *Annu Rev Med* 48: 307 – 316
31. Cannon B, Nedergaard J (2004) Brown adipose tissue: function and physiological significance. *Physiol Rev* 84: 277 – 359
32. Park U, Vastani N, Guan Y, Raja SN, Koltzenburg M, Caterina MJ (2011) TRP vanilloid 2 knock-out mice are susceptible to perinatal lethality but display normal thermal and mechanical nociception. *J Neurosci* 31: 11425 – 11436
33. You MH, Song MS, Lee SK, Ryu PD, Lee SY, Kim DY (2013) Voltage-gated K+ channels in adipogenic differentiation of bone marrow-derived human mesenchymal stem cells. *Acta Pharmacol Sin* 34: 129 – 136
34. Lefterova MI, Zhang Y, Steger DJ, Schupp M, Schug J, Cristancho A, Feng D, Zhuo D, Stoeckert CJ Jr, Liu XS *et al* (2008) PPARgamma and C/EBP factors orchestrate adipocyte biology via adjacent binding on a genome-wide scale. *Genes Dev* 22: 2941 – 2952
35. Nielsen R, Pedersen TA, Hagenbeek D, Moulos P, Siersbaek R, Megens E, Denissov S, Borgesen M, Francoijs KJ, Mandrup S *et al* (2008) Genome-wide profiling of PPARgamma:RXR and RNA polymerase II occupancy reveals temporal activation of distinct metabolic pathways and changes in RXR dimer composition during adipogenesis. *Genes Dev* 22: 2953 – 2967
36. Neal JW, Clipstone NA (2002) Calcineurin mediates the calcium-dependent inhibition of adipocyte differentiation in 3T3-L1 cells. *J Biol Chem* 277: 49776 – 49781
37. Cannon B, Nedergaard J (2011) Nonshivering thermogenesis and its adequate measurement in metabolic studies. *J Exp Biol* 214: 242 – 253
38. De Petrocellis L, Ligresti A, Moriello AS, Allara M, Bisogno T, Petrosino S, Stott CG, Di Marzo V (2011) Effects of cannabinoids and cannabinoid-enriched Cannabis extracts on TRP channels and endocannabinoid metabolic enzymes. *Br J Pharmacol* 163: 1479 – 1494
39. Kanzaki M, Zhang YQ, Mashima H, Li L, Shibata H, Kojima I (1999) Translocation of a calcium-permeable cation channel induced by insulin-like growth factor-I. *Nat Cell Biol* 1: 165 – 170
40. Boels K, Glassmeier G, Herrmann D, Riedel IB, Hampe W, Kojima I, Schwarz JR, Schaller HC (2001) The neuropeptide head activator induces activation and translocation of the growth-factor-regulated Ca(2+)-permeable channel GRC. *J Cell Sci* 114: 3599 – 3606
41. Sellayah D, Sikder D (2014) Orexin restores aging-related brown adipose tissue dysfunction in male mice. *Endocrinology* 155: 485 – 501
42. Wahlig JL, Bales ES, Jackman MR, Johnson GC, McManaman JL, Maclean PS (2012) Impact of high-fat diet and obesity on energy balance and fuel utilization during the metabolic challenge of lactation. *Obesity (Silver Spring)* 20: 65 – 75
43. Enerback S, Jacobsson A, Simpson EM, Guerra C, Yamashita H, Harper ME, Kozak LP (1997) Mice lacking mitochondrial uncoupling protein are cold-sensitive but not obese. *Nature* 387: 90 – 94
44. Katanosaka Y, Iwasaki K, Ujihara Y, Takatsu S, Nishitsuji K, Kanagawa M, Sudo A, Toda T, Katanosaka K, Mohri S *et al* (2014) TRPV2 is critical for the maintenance of cardiac structure and function in mice. *Nat Commun* 5: 3932
45. Motter AL, Ahern GP (2008) TRPV1-null mice are protected from diet-induced obesity. *FEBS Lett* 582: 2257 – 2262
46. Kusudo T, Wang Z, Mizuno A, Suzuki M (1985) Yamashita H (2012) TRPV4 deficiency increases skeletal muscle metabolic capacity and resistance against diet-induced obesity. *J Appl Physiol* 112: 1223 – 1232
47. Zhang Z, Zhang W, Jung DY, Ko HJ, Lee Y, Friedline RH, Lee E, Jun J, Ma Z, Kim F *et al* (2012) TRPM2 Ca2+ channel regulates energy balance and glucose metabolism. *Am J Physiol Endocrinol Metab* 302: E807 – E816
48. Hisanaga E, Nagasawa M, Ueki K, Kulkarni RN, Mori M, Kojima I (2009) Regulation of calcium-permeable TRPV2 channel by insulin in pancreatic beta-cells. *Diabetes* 58: 174 – 184
49. Hayato R, Higure Y, Kuba M, Nagai H, Yamashita H, Kuba K (2011) beta (3)-Adrenergic activation of sequential Ca(2+) release from mitochondria and the endoplasmic reticulum and the subsequent Ca(2+) entry in rodent brown adipocytes. *Cell Calcium* 49: 400 – 414
50. Thodeti CK, Matthews B, Ravi A, Mammoto A, Ghosh K, Bracha AL, Ingber DE (2009) TRPV4 channels mediate cyclic strain-induced endothelial cell reorientation through integrin-to-integrin signaling. *Circ Res* 104: 1123 – 1130
51. Cioffi DL (2007) The skinny on TRPV1. *Circ Res* 100: 934 – 936
52. Irie Y, Asano A, Canas X, Nikami H, Aizawa S, Saito M (1999) Immortal brown adipocytes from p53-knockout mice: differentiation and expression of uncoupling proteins. *Biochem Biophys Res Commun* 255: 221 – 225
53. Orr JS, Kennedy AJ, Hasty AH (2013) Isolation of adipose tissue immune cells. *J Vis Exp* 75: e50707
54. Brodie BB, Costa E, Dlabac A, Neff NH, Smookler HH (1966) Application of steady state kinetics to the estimation of synthesis rate and turnover time of tissue catecholamines. *J Pharmacol Exp Ther* 154: 493 – 498
55. Oi-Kano Y, Kawada T, Watanabe T, Koyama F, Watanabe K, Senbongi R, Iwai K (2013) Oleuropein supplementation increases urinary noradrenaline and testicular testosterone levels and decreases plasma corticosterone level in rats fed high-protein diet. *J Nutr Biochem* 24: 887 – 893
56. Young JB, Saville E, Rothwell NJ, Stock MJ, Landsberg L (1982) Effect of diet and cold exposure on norepinephrine turnover in brown adipose tissue of the rat. *J Clin Invest* 69: 1061 – 1071